TECHNICAL PAPER

Direct detection of wear conditions by classification of ferrograph images

Jingqiu Wang[1] · **Xinliang Liu**[1] · **Ming Wu**[1] · **Xiaolei Wang**[1]

Abstract

Wear particle analysis is one of the main indicators for the detection of wear condition. Traditional computer-aided wear particle analysis employs a unidirectional linear process, i.e. image preprocessing → wear particle segmentation → feature extraction → wear particle recognition → wear condition detection. It has disadvantages such as inaccurate segmentation of wear particles, numerous steps in the "artificial design feature method", accumulation and transmission of errors, and difficulty in overall optimization of the algorithms. In this study, a framework from overall determination to a detailed recognition is proposed to realize intelligent ferrography analysis. Furthermore, a convolutional neural network (CNN) is developed to classify seven types of ferrograph images, which can be used to directly determine wear conditions including initial wear, normal wear, abnormal wear, and severe wear. Compared with the traditional methods, the proposed CNN can automatically extract features layer by layer, yielding accurate end-to-end classification of the ferrograph images. The average accuracy of the CNN model on the test set is 90%. This research provides an effective solution for the automatic identification of wear conditions.

Keywords Wear particle analysis · Ferrography · Image classification · Convolutional neural network

1 Introduction

Wear debris generated from surface interaction is a relevant source of information on wear conditions and wear mechanisms. The commonly used techniques for wear particle analysis include ferrography, spectroscopy, and particle counting. Among these techniques, ferrography can be used to analyse the size, shape, colour, and texture of wear particles, which is beneficial for the detection of wear conditions.

Since the 1990s, ferrography has been developing towards automation [1–7] owing to the development of computer image processing. As shown in Fig. 1, the natural logical process to construct an automatic ferrography system is linear, including the following steps: image preprocessing → wear particle segmentation → feature extraction → wear particle recognition → wear condition detection. Various image processing techniques, such as image segmentation [8–11], feature extraction [12, 13], and classification methods [14–19], have been applied to wear particle analysis.

Although ferrography has achieved tremendous progress in automation, the following difficulties and challenges still exist:

- So far, no general or optimal algorithm has been developed to accurately segment deposited chains and blurred and overlapping wear particles.
- Feature parameters and recognition rules need to be designed and selected manually, as part of the "artificial design feature method". Some important feature parameters may be ignored, and some information may be redundant as well.
- Numerous steps in the linear flow may lead to accumulation and transmission of errors and a difficulty in overall optimization of the algorithm.

It is believed that "the human brain is the only known well-functioning visual system processing software". When an experienced analyst observes a ferrograph image, the wear

---

Technical Editor: Dr. Izabel Fernanda Machado.

✉ Jingqiu Wang
   meejqwang@nuaa.edu.cn

1 National Key Laboratory of Science and Technology on Helicopter Transmission, Nanjing University of Aeronautics and Astronautics, Nanjing 210016, China
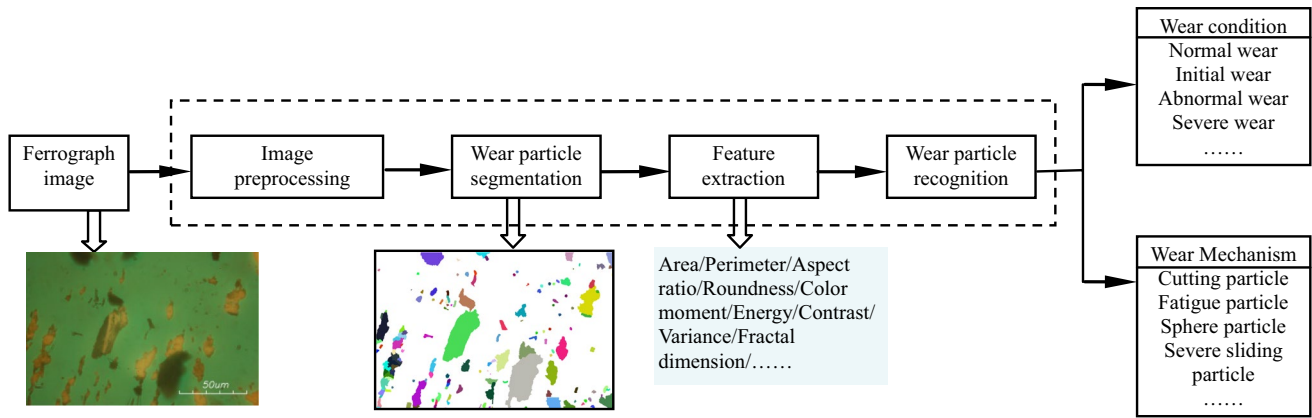
Fig. 1 Linear process of computer-aided ferrography analysis

condition can be identified or roughly "felt" simply by a glance. Subsequently, further observation is required to analyse whether or not large abnormal wear particles are present in the image. Further, the occurrence of scratches or pits on the particles needs to be determined. Moreover, the domination of serious sliding or fatigue wear in the image must be identified.

Hence, can we use reverse thinking once? Initially, images are classified to determine the wear conditions, and then, the "salient" or "sensitive" wear particles are identified, if necessary. Specifically, the process of automatic analysis of the wear condition is performed from the overall observations to achieve a detailed recognition.

The development of deep learning (DL) has provided the support to realize the above concept. In 2006, Hinton [20] proposed DL. A convolutional neural network (CNN) is one of the most well-known algorithms in DL; using images, it performs classification tasks directly. A CNN is composed of an end-to-end process, i.e. from the original image to the classification results; there are no intermediate steps, which is an important advantage compared to the previous linear classification methods.

CNN models such as AlexNet [21], GoogleNet [22], and SENet [23] have been proposed for image classification. These models need to be trained on large public datasets, such as ImageNet or MS COCO. Recently, Peng [24] used a CNN model to identify fatigue, oxide, and spherical particles, which provided a reference for the automatic analysis of the wear particles.

This study presents a new CNN model for the classification of ferrograph images which can be used for direct detection of the wear condition. Figure 2 shows the proposed process of the intelligent ferrography system. In this system, the CNN model can realize the classification of light, normal,
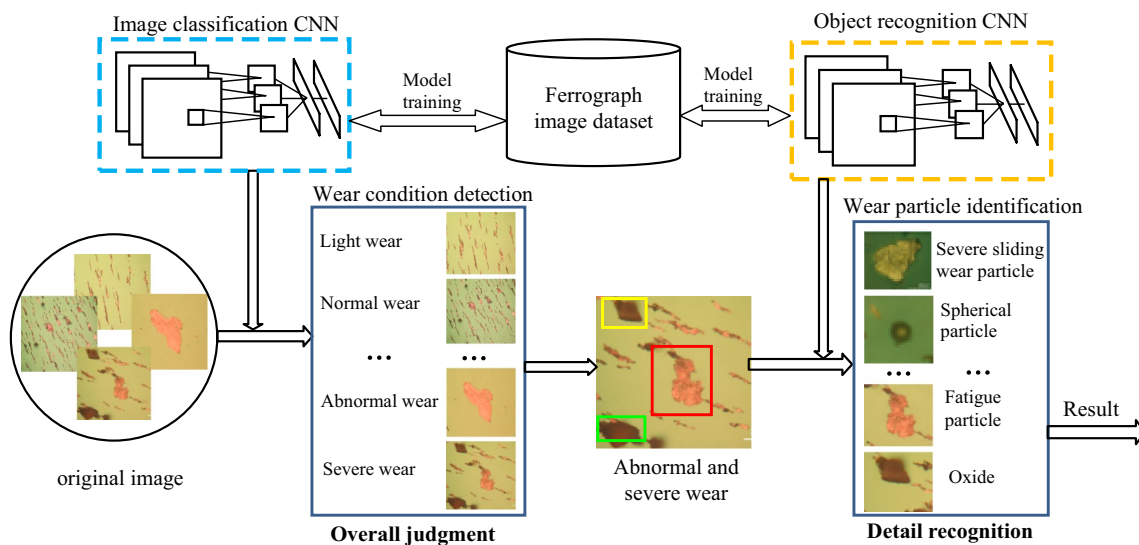

Fig. 2 Analysis process of the intelligent ferrography system

abnormal, and severe wear. For the images of abnormal and severe wear, a further identification CNN is performed for multi-object recognition to identify abnormal wear particles such as severe sliding, spherical, fatigue, and cutting wear particles. This study mainly introduces the construction of a CNN model for the classification of ferrograph images.

2 Proposed CNN for the classification of ferrograph images

Until now, no rules have been formulated to be followed for architecture construction and parameter settings of a CNN model, and the internal mechanisms of a CNN model such as self-learning and transmission of features are still unclear. Hence, while constructing the CNN for wear particle image classification, we adopt the strategies discussed in the following section.

2.1 Construction strategy of the CNN model

- Reduce the network depth

Generally, a CNN model with a deeper network has features with a strong learning ability. In this study, the ferrograph images were classified into seven categories based on the different wear conditions. Therefore, choosing the appropriate depth was of tremendous importance to reduce the network size and image processing time, thereby improving the processing efficiency.

- Reduce the size of convolutional kernels

A large convolution kernel is associated with good local feature extraction and high learning ability of the model.

However, owing to the complexity of the calculation, numerous training parameters are needed, and overfitting is prone to occur. Thus, using small convolution kernels is conducive to reduce the size of a CNN model.

- Reduce the number of input and output channels

For a convolution layer with a convolution kernel size of $K \times K$, the number of parameters of the current convolution layer can be calculated without considering bias.

$$S = K \times K \times I \times O \tag{1}$$

where I is the number of input channels and O is the number of output channels, and more channels imply more feature maps. To reduce the size of a CNN model, not only the size of the convolution kernels but also the number of input and output channels should be reduced.

- Dataset with appropriate number of images and category balance

The number and diversity of the image samples have a direct impact on the performance of a CNN model. Thus, to develop a CNN for the classification of ferrograph images, it is necessary to construct a dataset containing sufficient number of ferrograph images and typical categories as well as to ensure that the numbers of different categories of images are balanced.

2.2 Architecture of the proposed CNN

Based on the above strategy, a new CNN was constructed to realize the direct detection of different wear conditions. Figure 3 shows its overall architecture. The CNN model contains an input layer, four convolutional units (UnitConv1 to
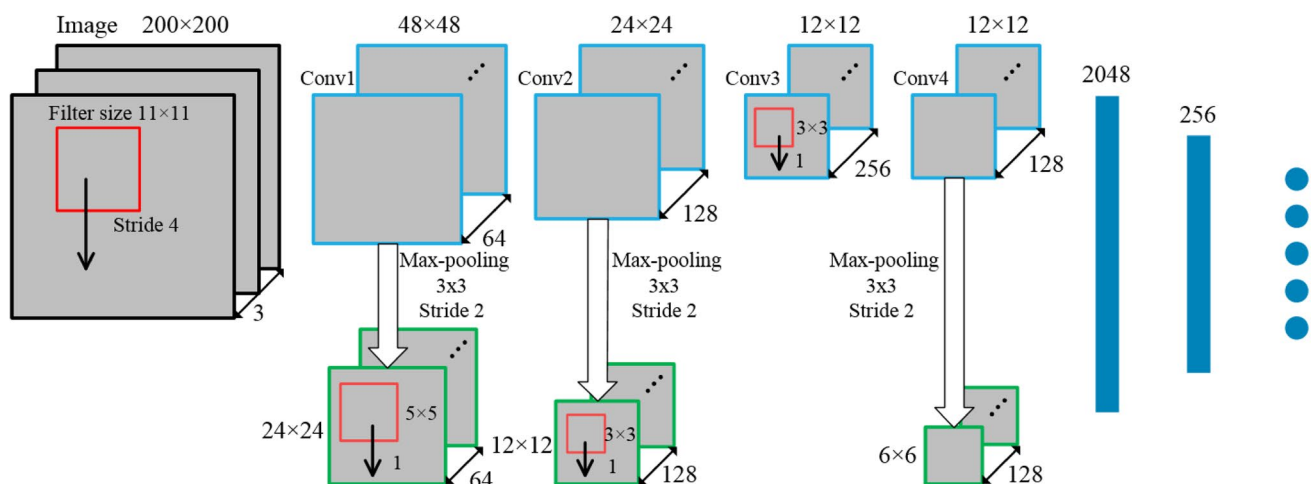

Fig. 3 Overall architecture of the proposed CNN

UnitConv4), two fully connected layers (Fc1, Fc2), and an output layer. Each convolutional unit consists of a convolution layer and a max-pooling layer, as shown in Fig. 4.

Table 1 lists the architecture parameters of the proposed CNN. In Table 1, W, H, and C represent the width,

height, and number of a feature map, respectively. The input of the CNN is a ferrograph image of size 200×200. UnitConv1 adopts the traditional convolution form, which includes one convolution layer and one pooling layer. In addition, each convolution layer is followed by a rectified
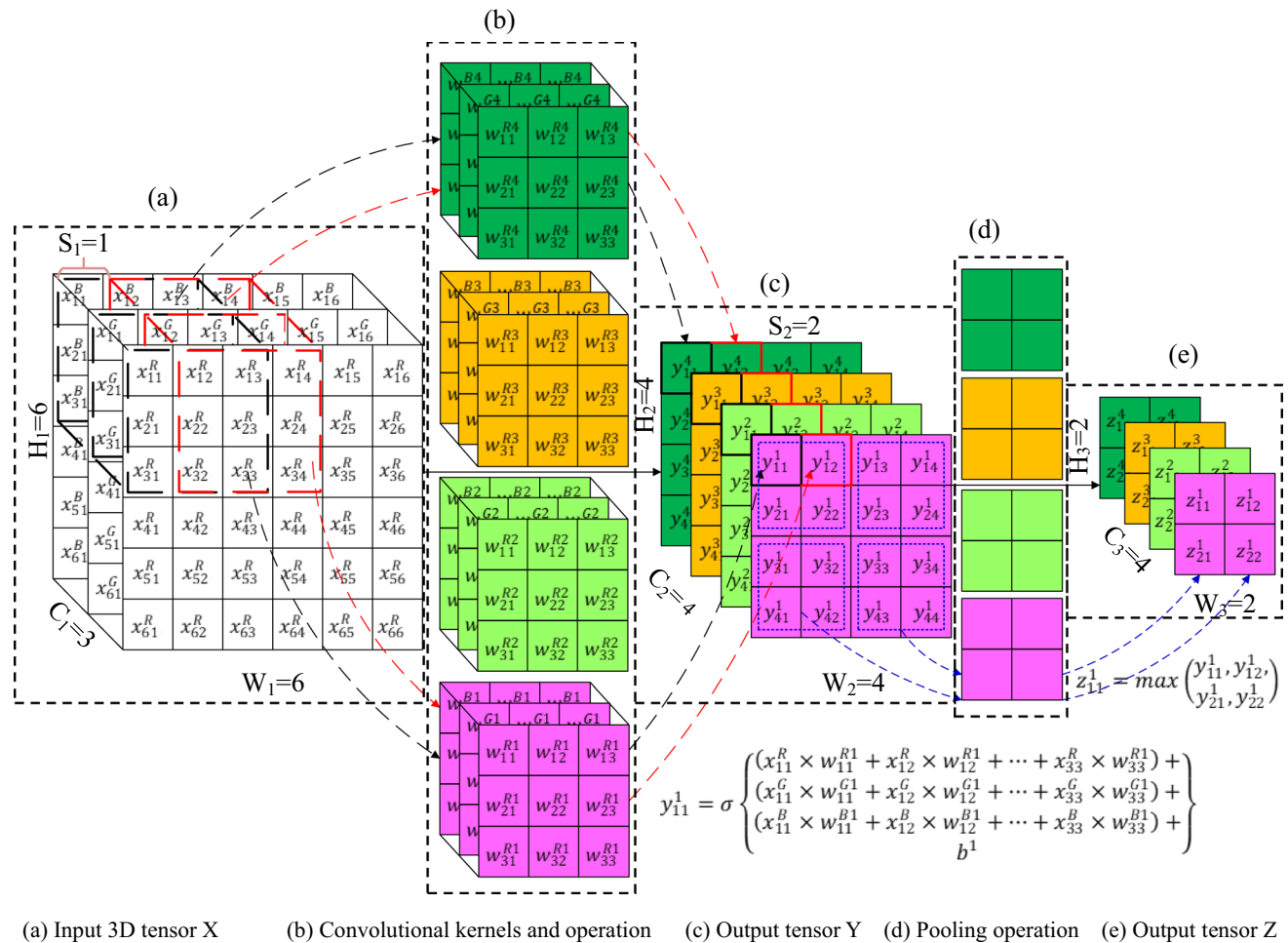

(a) Input 3D tensor X   (b) Convolutional kernels and operation   (c) Output tensor Y   (d) Pooling operation   (e) Output tensor Z

Fig. 4 Convolution and max-pooling operations

Table 1 Architecture parameters of the CNN model

Structure units	Layer name	Operation	Kernel/stride/zero-padding	Output ($W \times H \times C$)
Input	Data	Data	–	$200 \times 200 \times 3$
UnitConv1	Conv1	Convolution	$11 \times 11/4/0$	$48 \times 48 \times 64$
	Pool1	Max-pooling	$3 \times 3/2/0$	$24 \times 24 \times 64$
UnitConv2	Conv2	Convolution	$5 \times 5/1/4$	$24 \times 24 \times 128$
	Pool2	Max-pooling	$3 \times 3/2/0$	$12 \times 12 \times 128$
UnitConv3	Conv3	Convolution	$3 \times 3/1/0$	$12 \times 12 \times 256$
UnitConv4	Conv4	Convolution	$3 \times 3/1/2$	$12 \times 12 \times 128$
	Pool4	Max-pooling	$3 \times 3/2/0$	$6 \times 6 \times 128$
UnitFc	Fc1	InnerProduct	–	2048
	Fc2	InnerProduct	–	256

linear unit (ReLU) layer [21] to enhance the nonlinear fitting ability of the CNN model.

As summarized in Table 1, except for UnitConv3, which has no pooling operation, the other three units have the same structure but with different sizes of the kernels, strides, and zero-padding operations. From UnitConv1 to UnitConv4, the sizes of convolution kernels decrease gradually, in the order: 11×11, 5×5, 3×3, and 3×3. Zero-padding operations are needed for convolution kernels whose sizes are 5×5 or 3×3. For UnitConv2, before the convolution operation, the size of the feature map is 24×24 and it is enlarged to 28×28 by the zero-padding operation. For UnitConv4, the size of the feature map is 12×12, which is enlarged to 14×14. Thus, the size of the feature map does not change after convolution. The pooling layer adopts the max-pooling operation, and the size of pooling kernel is 3×3, and its stride is 2. After the pooling operation, the size of the feature map is reduced by half to achieve dimension reduction.

The proposed CNN has four convolutional layers. The first layer has 64 convolution kernels, which implies that this layer has 64 output feature maps. The second, third, and fourth convolution layers have 128, 256, and 128 kernels, respectively. Because the convolution kernels used in the CNN are small, the CNN parameters are effectively reduced.

After the last pooling of UnitConv4, all the parameters are input to the first fully connected layer, which has 2048 neurons and then to the second fully connected layer, which has 256 neurons. Finally, using the Softmax activation function, the probability of the image category is obtained. The maximum probability represents the category of the ferrograph image. In addition, the fifth and sixth fully connected layers use Dropout [25] with a probability of 0.5 in the training process.

By using the above architecture construction and parameter setting, a miniaturized CNN model for ferrograph image classification was developed.

3 Experiments

Under a stable wear condition, wear debris is small and they deposit on the ferrogram in the form of chains. With an increase in the wear rate, the densities of the wear particles or chains as well as the particle size increase. When severe wear occurs owing to the different wear modes, block particles, including fatigue and severe sliding particles, cutting particles, spherical wear particles, and other types may appear in the image. Different types of wear particles may be observed simultaneously in an image, such as wear particle chains and fatigue block particles, or chain and cutting wear particles, which indicate the possibility of abnormal wear.
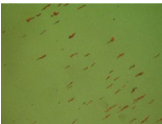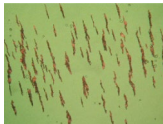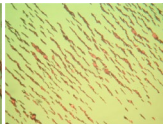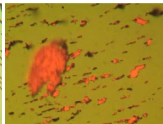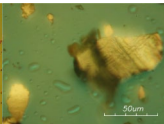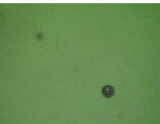
Therefore, in our experiments, the ferrograph images are divided into seven categories based on the wear conditions, as listed in Table 2.

All the images in our experiments were captured from mining and petrochemical equipment. The ferrograph image dataset included a training set, validation set, and test set. The training set is used to optimize the parameter of CNN model, and the validation set allows us to evaluate the model so as to select the best architecture. The test set is used for the final evaluation at the end of the model development, to see how the model performs on unseen data, that is, to illustrate the generalization ability of the CNN model. The number of image samples in the three sets was 28,000, 7000, and 3500, respectively. The images of each category in the same dataset were identical.

3.1 Experimental results and analysis

All the experiments were run on a caffe platform and a NVIDIA GTX 1070 8G GPU. During the training process, some hyper-parameters were needed to be set, including batch size, momentum, and learning rate, etc. The main role of batch size is to determine the gradient direction. The momentum can effectively modify the descent direction and step of the gradient. The learning rate determines how "quickly" the gradient updates follow the gradient direction.

Table 2 Different categories of original ferrograph images

Image sample							
Category	S-chains (a few fine particles appear as chains)	M-chains (a medium number of particles appear as chains)	L-chains (numerous particles deposited as chains)	Multi-type wear particles	Block wear particles	Cutting wear particles	Spherical wear particles
Wear condition	Light wear	Normal wear	Abnormal wear	Severe wear	Severe wear	Abnormal wear	Abnormal wear

In this study, the random gradient descent algorithm with a batch size of 128 and momentum of 0.9 was used. The learning rate was set as 0.001, and the learning rate decay was set as 0.1.

Two experiments were implemented to verify the efficiency of the proposed CNN.

3.1.1 Classification efficiency of the CNN

The architecture and parameters of a CNN model have a major influence on its classification efficiency. The number of layers and channels not only affect the classification results but also the size of the model. Therefore, we compared the classification efficiencies of models with different architectures on the validation set. Classification efficiency refers to the time consumed for image classification, i.e. the average time required for the forward calculation of an image on the caffe platform. The size of a model is the number of parameters of the CNN model trained on the caffe platform, and the smaller the model, the smaller the memory space required. The results are listed in Table 3.

It can be seen from Table 3 that the CNN models have different numbers of convolution layers or kernels. The highest accuracy is associated with the second model, which has five layers. With the simplification of the structure, the processing time per image is gradually reduced and the size of the model is also gradually decreased. The accuracy of the fifth model is 98.85%, with a processing time per image of 6.47 ms. However, if the number of network layers is further reduced, such as in the sixth model, which has only three layers, the classification accuracy rate decreases to 97.93%. Therefore, by weighing the classification accuracy and efficiency, the fifth model has the best architecture, which is the architecture of the proposed CNN.

Figure 5 shows the accuracy and loss curve of the CNN on the validation set. After 3000 iterations of training and learning, the classification accuracy rate is 98.85%.

To verify the validity of the CNN model, it was compared with contemporary models including AlexNet and VGG16.

Table 3 Comparison of the CNN models having different architectures

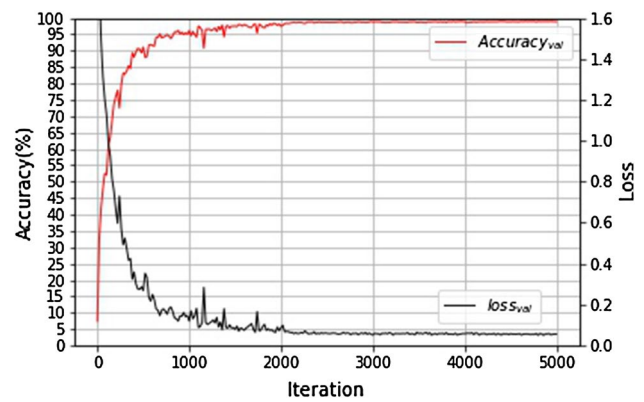| No	Architectures	Accuracy (%)	Efficiency (ms/image)	Size of model (MB)
1	96-128-256-384-384-256	98.68	7.38	83.7
2	96-256-384-384-256	98.93	7.23	82.9
3	64-128-256-256-128	98.71	6.73	41.3
4	96-128-256-128	98.73	6.53	40.4
5	64-128-256-128	98.85	6.47	40.1
6	64-128-128	97.93	6.37	39

Fig. 5 Training curve on the validation set

Table 4 summarizes the classification efficiencies and model sizes of the three CNNs on the validation set.

It can be deduced from Table 4 that the proposed CNN has a slightly higher rate of classification accuracy than the other two models. Moreover, its efficiency is 6.47 ms per image, which is improved by 24% and 60%, respectively, in comparison with the other two CNNs. Additionally, the size of the proposed CNN is only 40.1 MB, much smaller than the other two models.

3.1.2 Classification accuracy

The accuracy of the CNN was assessed on a test set. Some ferrograph images of different types were selected randomly from the test set and are shown in Fig. 6. These include the chains from a small number of particles to a large number of particles, multi-type (chain + block, blocks, sphere + block, chain + block + cutting) particles, block, cutting and spherical wear particles, respectively.

Each column in Table 5 corresponds to the classification results for each image. The value represents the probability of the image belonging to the corresponding category. The maximum value is considered as the most probable category of the image. The probability that Fig. 6a has a small number of chain particles is 97.5%, and the probability that Fig. 6j has a sphere particle is 100%, much higher than the probabilities for the other categories.

Table 4 CNN performances on the validation set

Model	Accuracy (%)	Efficiency (ms/image)	Size of model (MB)
AlexNet	98.51	8.56	217
VGG16	98.29	16.17	512
CNN	98.85	6.47	40.1

(a) S-Chain　　**(b)** M-Chain　　**(c)** L-Chain　　**(d)** Multi-type　　**(e)** Multi-type

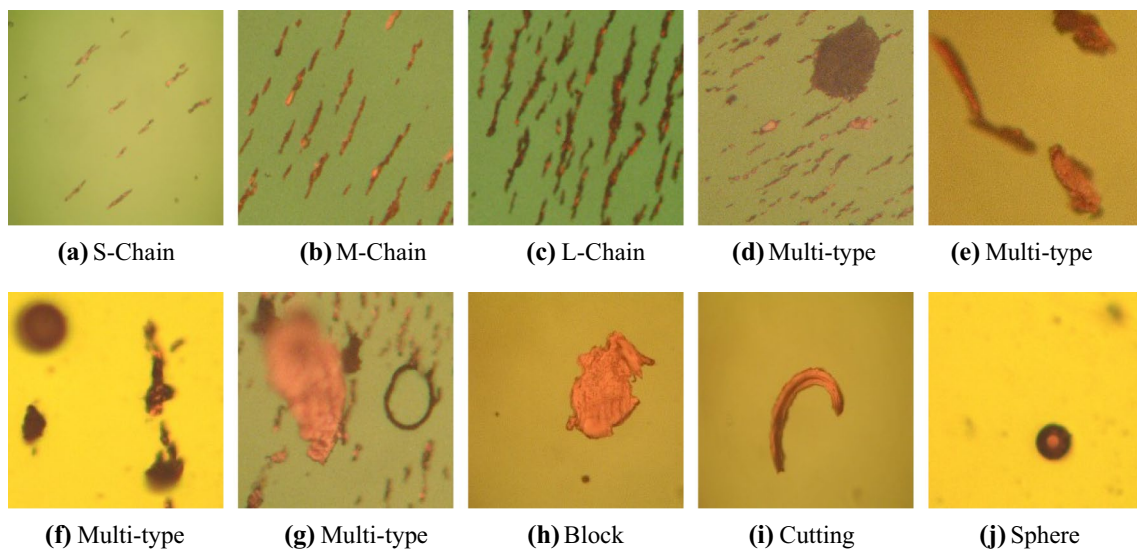**(f)** Multi-type　　**(g)** Multi-type　　**(h)** Block　　**(i)** Cutting　　**(j)** Sphere

Fig. 6 Examples in each category

Table 5 Classification results of the wear particle images

Classification (probability %)	Fig. 6a	Fig. 6b	Fig. 6c	Fig. 6d	Fig. 6e	Fig. 6f	Fig. 6g	Fig. 6h	Fig. 6i	Fig. 6j
S-Chain	97.5	0.04	0.00	0.00	0.00	0.00	0.00	0.00	0.00	0.00
M-Chain	2.35	99.96	0.08	0.00	0.00	0.00	0.00	0.00	0.00	0.00
L-Chain	0.00	0.00	99.92	0.00	0.00	0.00	0.00	0.00	0.00	0.00
Multi-type	0.01	0.00	0.00	99.81	99.91	100	100	0.00	0.00	0.00
Block	0.01	0.00	0.00	0.19	0.00	0.00	0.00	100	0.00	0.00
Cutting	0.06	0.00	0.00	0.00	0.09	0.00	0.00	0.00	100	0.00
Sphere	0.07	0.00	0.00	0.00	0.00	0.00	0.00	0.00	0.00	100

Table 6 Classification accuracy of the CNNs

Type	CNN	HOG + SURF + SVM
Few chains	99.4	76
Medium number of chains	96.8	
Numerous of chains	99.6	
Multi-type	92.4	66
Block	91.0	72
Cutting	95.4	64
Sphere	97.6	80
Average	96.0	71.6

For the ten images in Fig. 6, the classification results are consistent with the actual type.

Table 6 lists for all the 3500 images in the test set, the classification accuracies using the proposed CNN, and the traditional classification method of support vector machine (SVM).

Although the classification results of the CNN on the test set are lower than those obtained on the validation set, the average accuracy rate is still higher than 90%. Among them, the classification accuracy of the image with numerous chain particles is the highest, which is 99.6%. This may be because the visual saliency of the chain particles is the most significant. The classification accuracy of block particles is 91%, which is the lowest. This is because of the irregularity of block particles and their large proportion in multi-type images, so that they can be easily misclassified as spherical or multi-type images. In general, the test results show that the CNN model has the characteristics of simple processing and high classification accuracy.

In addition, we compared the proposed CNN with the traditional classification method of SVM. The feature extraction operator, histogram of oriented gradients (HOG), and speeded up robust features (SURF) were combined to extract the features of the wear particles, and then, an SVM was used to realize the classification of the ferrograph images. As summarized in Table 6, the average classification accuracy of the SVM is 71.6%, which is lower than that of the CNN proposed in this study. It is noted that the HOG and SURF operators are directly used

on the original image, without the segmentation process of the wear particles.

3.2 Visualization of the output of each layer of the CNN model

To further illustrate the validity of the CNN, the output feature maps of each convolution layer were visualized and analysed. Additionally, the t-distributed stochastic neighbour embedding (T-SNE) [26] algorithm was used to analyse the output of the last fully connected layer.

3.2.1 Visualization of the feature maps of each convolutional layer

In view of the black-box nature of the CNN in feature extraction, the output feature maps of each layer were visualized to exhibit the results of the convolutional operation.

Figure 7a shows an original image of a fatigue particle, and Fig. 7b–e presents the feature maps extracted from all the four convolutional layers. The first convolutional layer outputs 64 feature maps, each of size 48×48, which are displayed in grey form in Fig. 7b. According to the CNN architecture, 128, 256, and 128 feature maps are output from the second, third, and fourth layers, respectively, and the corresponding sizes of each feature map are 24×24, 12×12, and 12×12.

Figure 7 shows that the features extracted from each layer are different. The first layer yields images of the wear particles with different brightness and their fine edges. Therefore, this layer has the functions of removing the background, extracting the particle shape, and locating the wear particles. The second layer mainly extracts some of the rough edges

of the wear particles. In addition to extracting the features of the former layer, it can also be regarded to be concerned with the local features of the wear particles. The third layer has numerous convolution kernels, and the highlighted parts of numerous feature maps cover almost all the wear particles. It can be understood that this layer not only continues to extract the features of the previous layer but also mainly realizes the extraction of the wear particle textures. The last layer includes a few convolution kernels. The main function of this layer is to represent the wear particles with few distinguished parameters at a high-dimensional level.

Figure 8 shows the feature maps of four block particles. Figure 8a presents their original images. Figure 8b–e shows the feature maps after a convolution operation performed by the same convolution kernel in each convolution layer. It can be found that in a specific convolution layer, the response of the same convolution kernel to the same type of wear particle is consistent.

Therefore, the different convolution layers realize the extraction of the wear particle features in a stepwise manner. Simultaneously, the contributions of the different convolution kernels in each layer to the feature extraction are different, and finally, the features that can be used to classify wear particles are extracted.

3.2.2 Visualization of the features output from the last fully connected layer

To further illustrate the efficiency of the proposed CNN model, the T-SNE algorithm was used to visualize the output of the final fully connected layers of AlexNet, VGG16, and the proposed CNN model, as shown in Fig. 9. In each of the seven categories of the ferrograph images,
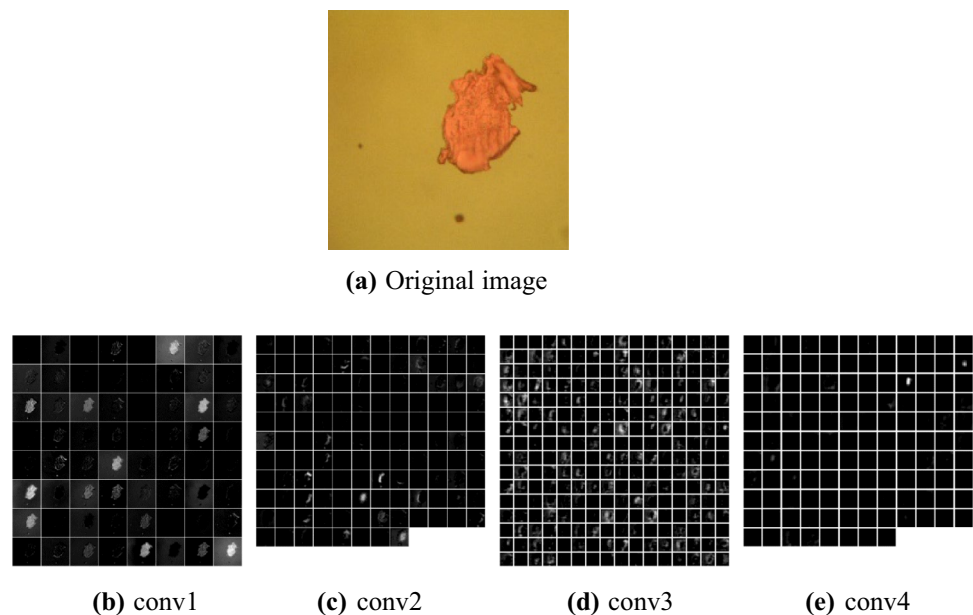
Fig. 7 Feature maps of the convolutional layers

(a) Original image

(b) conv1   **(c)** conv2   **(d)** conv3   **(e)** conv4

Fig. 8 Feature maps of the same convolutional kernels for the same types of wear particles

(a) Original image

(b) Conv 1

(c) Conv 2

(d) Conv 3

(e) Conv 4

(a) AlexNet

(b) VGG16

(c) Proposed CNN

- Sphere
- Cutting
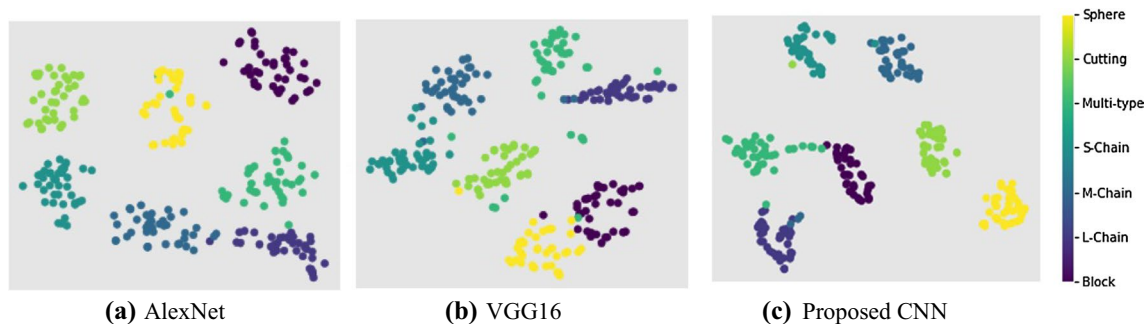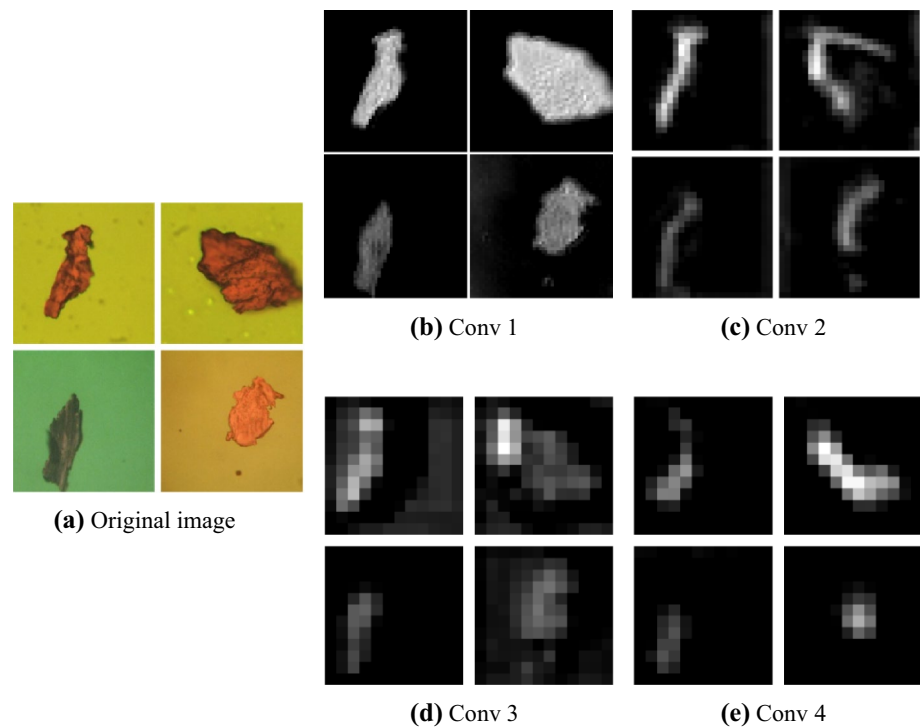- Multi-type
- S-Chain
- M-Chain
- L-Chain
- Block

Fig. 9 Visualization of the feature vector in the fully connected layer by t-SNE

40 samples were selected randomly. In Fig. 9, a small dot represents an image sample, and the samples of the same category are clustered together, and the different type ones are scattered from each other.

In Fig. 9a, b, all the types of samples display a clustering trend; similar samples are clustered but relatively loosely, i.e. the distances between the clusters are not sufficiently long by AlexNet. Figure 9c is the visualization result of the CNN. It can be seen that compared with the other models, the CNN has a stronger recognition ability for the samples belonging to the same category. Simultaneously, the distances between different clusters are relatively larger, which suggests that the model has better discrimination ability when the categories are different.

Therefore, the proposed CNN model can automatically extract features layer by layer, yielding accurate end-to-end classification of the ferrograph images.

4 Conclusion

Developing algorithms that take advantages of human visual inspection is still a challenging task. In this study, a framework from overall determination to a detailed recognition is proposed to realize intelligent ferrography analysis. Furthermore, a CNN model is constructed for the classification of seven types of ferrograph images, and thus, the wear conditions can be directly detected based on the category

of a ferrograph image. The experimental results show that the average accuracy of the proposed CNN on the test set is approximately 90%, higher than the value obtained in conventional ferrograph image classification methods. The CNN model can process each image at a speed of 6.47 ms, so that it can be used for online or offline ferrography image detection.

References

1. Roylance BJ (2005) Ferrography—then and now. Tribol Int 38(10):857–862
2. Kumar M (2013) Advancement and current status of wear debris analysis for machine condition monitoring: a review. Ind Lubr Tribol 65(1):3–11
3. Gonçalves VD, Almeida LF, Mathias MH (2010) Wear particle classifier system based on an artificial neural network. J Mech Eng 56:284–289
4. Laghari M, Ahmed F (2009) Wear particle profile analysis. In: 2009 international conference on signal processing systems, Singapore, pp 546–550
5. Myshkin NK, Grigoriev AY (2008) Morphology: texture, shape, and color of friction surfaces and wear debris in tribodiagnostics problems. J Frict Wear 29(3):192–199
6. Stachowiak GW, Podsiadlo P (2006) Towards the development of an automated wear particle classification system. Tribol Int 39(12):1615–1623
7. Raadnui S (2005) Wear particle analysis—utilization of quantitative computer image analysis: a review. Tribol Int 38(10):871–878
8. Wang J, Zhang L, Lu F et al (2014) The segmentation of wear particles in ferrograph images based on an improved ant colony algorithm. Wear 311(1–2):123–129
9. Wu H, Wu T, Peng Y et al (2014) Watershed-based morphological separation of wear debris chains for on-line ferrograph analysis. Tribol Lett 53(2):411–420
10. Wang J, Zhang L, Wang X (2013) Combining k-means clustering and watershed algorithm for the segmentation of color ferrograph image. J China Univ Minning Technol 42(5):866–872
11. Hu X, Huang P, Zheng S (2007) On the pretreatment process for the object extraction in color image of wear debris. Int J Imaging Syst Technol 17(5):277–284
12. Stachowiak GP, Podsiadlo P, Stachowiak GW (2006) Shape and texture features in the automated classification of adhesive and abrasive wear particles. Tribol Lett 24(1):15–26
13. Myshkin NK, Kong H, Grigoriev AY et al (2001) The use of color in wear debris analysis. Wear 251:1218–1226
14. Myshkin NK, Kwon OK, Grigoriev AY et al (1997) Classification of wear debris using a neural network. Wear 203–204:658–662
15. Peng Z, Kirk TB (1998) Automatic wear particle classification using neural networks. Tribol Lett 5:249–257
16. Yan XP, Zhao CH, Lu ZY et al (2005) A study of information technology used in oil monitoring. Tribol Int 38(10):879–886
17. Chen S, Li Z, Xu Q (2006) Grey target theory based equipment condition monitoring and wear mode recognition. Wear 260(4–5):438–449
18. Li Q, Zhao T, Zhang L et al (2017) Ferrography wear particles image recognition based on extreme learning machine. J Electr Comput Eng 2017:1–6
19. Yuan W, Chin KS, Hua M et al (2016) Shape classification of wear particles by image boundary analysis using machine learning algorithms. Mech Syst Signal Process 72–73:346–358
20. Hinton GE, Salakhutdinov RR (2006) Reducing the dimensionality of data with neural networks. Science 313:504–507
21. Krizhevsky A, Sutskever I, Hinton GE (2012) Imagenet classification with deep convolutional neural networks. In: Proceedings of advances in neural information processing systems South Lake Tahoe, USA, IEEE Press, pp 1097–1105
22. Szegedy C, Liu W, Jia Y et al (2015) Going deeper with convolutions. In: Proceedings of the 2015 IEEE conference on computer vision and pattern recognition, Boston, MA, IEEE, pp 1–9
23. Hu J, Shen L, Albanie S et al (2017) Squeeze-and-Excitation networks. arXiv:1709.01507
24. Peng P and Wang J (2019) Wear particle classification considering particle overlapping. Wear 422–423:119–127
25. Srivastava N, Hinton G, Krizhevsky A et al (2014) Dropout: a simple way to prevent neural networks from overfitting. J Mach Learn Res 15:1929–1958
26. Maaten L, Hinton G (2008) Visualizing data using t-SNE. J Mach Learn Res 9:1–48